EUROPEAN ORGANISATION FOR PARTICLE PHYSICS

CERN–PPE/94–52
18 March 1994

A study of mean sub-jet multiplicities in two- and three-jet hadronic Z^0 decays

The OPAL Collaboration

Abstract

This paper describes an analysis of sub-jet multiplicities, which are expected to be sensitive to the properties of soft gluon radiation, in hadronic decays of the Z^0. Two- and three-jet event samples are selected using the $k_\perp$ jet clustering algorithm at a jet resolution scale y_1. The mean sub-jet multiplicity as a function of the sub-jet resolution, y_0, is determined separately for both event samples by reapplying the same jet algorithm at resolution scales $y_0 < y_1$. These measurements are compared with recent perturbative QCD calculations based on the summation of leading and next-to-leading logarithms, and with QCD Monte Carlo models. The analytic calculations provide a good description of the sub-jet multiplicity seen in three- and two-jet events in the perturbative region ($y_0 \sim y_1$), and the measured form of the data is in agreement with the expectation based on coherence of soft gluon radiation. The analysis provides good discrimination between Monte Carlo models, and those with a coherent parton shower are preferred by the data. The analysis suggests that coherence effects are present in the data.

(Submitted to Zeitschrift für Physik C)

The OPAL Collaboration

R. Akers[16], G. Alexander[23], J. Allison[16], K.J. Anderson[9], S. Arcelli[2], S. Asai[24], A. Astbury[28], D. Axen[29], G. Azuelos[18,a], A.H. Ball[17], R.J. Barlow[16], S. Barnett[16], R. Bartoldus[3], J.R. Batley[5], G. Beaudoin[18], A. Beck[23], G.A. Beck[13], J. Becker[10], C. Beeston[16], T. Behnke[27], K.W. Bell[20], G. Bella[23], P. Bentkowski[18], P. Berlich[10], S. Bethke[32], O. Biebel[3], I.J. Bloodworth[1], P. Bock[11], B. Boden[3], H.M. Bosch[11], M. Boutemeur[18], P. Bright-Thomas[25], R.M. Brown[20], A. Buijs[8], H.J. Burckhart[8], C. Burgard[27], P. Capiluppi[2], R.K. Carnegie[6], A.A. Carter[13], J.R. Carter[5], C.Y. Chang[17], C. Charlesworth[6], D.G. Charlton[8], S.L. Chu[4], P.E.L. Clarke[15], J.C. Clayton[1], I. Cohen[23], J.E. Conboy[15], M. Cooper[22], M. Coupland[14], M. Cuffiani[2], S. Dado[22], C. Dallapiccola[17], G.M. Dallavalle[2], C. Darling[31], S. De Jong[13], L.A. del Pozo[5], H. Deng[17], M. Dittmar[4], M.S. Dixit[7], E. do Couto e Silva[12], J.E. Duboscq[8], E. Duchovni[26], G. Duckeck[8], I.P. Duerdoth[16], D.J.P. Dumas[6], P.A. Elcombe[5], P.G. Estabrooks[6], E. Etzion[23], H.G. Evans[9], F. Fabbri[2], B. Fabbro[21], M. Fierro[2], M. Fincke-Keeler[28], H.M. Fischer[3], R. Folman[26], D.G. Fong[17], M. Foucher[17], H. Fukui[24], A. Fürtjes[8], A. Gaidot[21], J.W. Gary[4], J. Gascon[18], N.I. Geddes[20], C. Geich-Gimbel[3], S.W. Gensler[9], F.X. Gentit[21], T. Geralis[20], G. Giacomelli[2], P. Giacomelli[4], R. Giacomelli[2], V. Gibson[5], W.R. Gibson[13], J.D. Gillies[20], J. Goldberg[22], D.M. Gingrich[30,a], M.J. Goodrick[5], W. Gorn[4], C. Grandi[2], F.C. Grant[5], J. Hagemann[27], G.G. Hanson[12], M. Hansroul[8], C.K. Hargrove[7], P.F. Harrison[13], J. Hart[8], P.A. Hart[9], P.M. Hattersley[1], M. Hauschild[8], C.M. Hawkes[8], E. Heflin[4], R.J. Hemingway[6], G. Herten[10], R.D. Heuer[8], J.C. Hill[5], S.J. Hillier[8], T. Hilse[10], D.A. Hinshaw[18], P.R. Hobson[25], D. Hochman[26], R.J. Homer[1], A.K. Honma[28,a], R.E. Hughes-Jones[16], R. Humbert[10], P. Igo-Kemenes[11], H. Ihssen[11], D.C. Imrie[25], A. Jawahery[17], P.W. Jeffreys[20], H. Jeremie[18], M. Jimack[1], M. Jones[6], R.W.L. Jones[8], P. Jovanovic[1], C. Jui[4], D. Karlen[6], K. Kawagoe[24], T. Kawamoto[24], R.K. Keeler[28], R.G. Kellogg[17], B.W. Kennedy[15], J. King[13], S. Kluth[5], T. Kobayashi[24], M. Kobel[10], D.S. Koetke[8], T.P. Kokott[3], S. Komamiya[24], R. Kowalewski[8], R. Howard[29], J. von Krogh[11], J. Kroll[9], P. Kyberd[13], G.D. Lafferty[16], H. Lafoux[8], R. Lahmann[17], J. Lauber[8], J.G. Layter[4], P. Leblanc[18], P. Le Du[21], A.M. Lee[31], E. Lefebvre[18], M.H. Lehto[15], D. Lellouch[26], C. Leroy[18], J. Letts[4], L. Levinson[26], Z. Li[12], S.L. Lloyd[13], F.K. Loebinger[16], G.D. Long[17], B. Lorazo[18], M.J. Losty[7], X.C. Lou[8], J. Ludwig[10], A. Luig[10], M. Mannelli[8], S. Marcellini[2], C. Markus[3], A.J. Martin[13], J.P. Martin[18], T. Mashimo[24], P. Mättig[3], U. Maur[3], J. McKenna[29], T.J. McMahon[1], J.R. McNutt[25], F. Meijers[8], F.S. Merritt[9], H. Mes[7], A. Michelini[8], R.P. Middleton[20], G. Mikenberg[26], J. Mildenberger[6], D.J. Miller[15], R. Mir[12], W. Mohr[10], C. Moisan[18], A. Montanari[2], T. Mori[24], M. Morii[24], U. Müller[3], B. Nellen[3], H.H. Nguyen[9], S.W. O'Neale[1], F.G. Oakham[7], F. Odorici[2], H.O. Ogren[12], C.J. Oram[28,a], M.J. Oreglia[9], S. Orito[24], J.P. Pansart[21], P. Paschievici[26], G.N. Patrick[20], M.J. Pearce[1], P. Pfister[10], J.E. Pilcher[9], J. Pinfold[30], D. Pitman[28], D.E. Plane[8], P. Poffenberger[28], B. Poli[2], T.W. Pritchard[13], H. Przysiezniak[18], G. Quast[27], M.W. Redmond[8], D.L. Rees[8], G.E. Richards[16], M. Rison[5], S.A. Robins[13], D. Robinson[5], A. Rollnik[3], J.M. Roney[28], E. Ros[8], S. Rossberg[10], A.M. Rossi[2], M. Rosvick[28], P. Routenburg[30], K. Runge[10], O. Runolfsson[8], D.R. Rust[12], M. Sasaki[24], C. Sbarra[2], A.D. Schaile[26], O. Schaile[10], F. Scharf[3], P. Scharff-Hansen[8], P. Schenk[4], B. Schmitt[3], H. von der Schmitt[11], M. Schröder[12], H.C. Schultz-Coulon[10], P. Schütz[3], M. Schulz[8], C. Schwick[27], J. Schwiening[3], W.G. Scott[20], M. Settles[12], T.G. Shears[5], B.C. Shen[4], C.H. Shepherd-Themistocleous[7], P. Sherwood[15], G.P. Siroli[2], A. Skillman[16], A. Skuja[17], A.M. Smith[8], T.J. Smith[28], G.A. Snow[17], R. Sobie[28], R.W. Springer[17], M. Sproston[20], A. Stahl[3], C. Stegmann[10], K. Stephens[16], J. Steuerer[28], R. Ströhmer[11], D. Strom[19], H. Takeda[24], S. Tarem[8], M. Tecchio[9], P. Teixeira-Dias[11], N. Tesch[3],

M.A. Thomson[15], E. Torrente-Lujan[22], S. Towers[6], N.J. Tresilian[16], T. Tsukamoto[24], M.F. Turner[8], D. Van den plas[18], R. Van Kooten[12], G.J. VanDalen[4], G. Vasseur[21], M. Vincter[28], A. Wagner[27], D.L. Wagner[9], C. Wahl[10], C.P. Ward[5], D.R. Ward[5], J.J. Ward[15], P.M. Watkins[1], A.T. Watson[1], N.K. Watson[7], P. Weber[6], P.S. Wells[8], N. Wermes[3], B. Wilkens[10], G.W. Wilson[4], J.A. Wilson[1], V-H. Winterer[10], T. Wlodek[26], G. Wolf[26], S. Wotton[11], T.R. Wyatt[16], R. Yaari[26], A. Yeaman[13], G. Yekutieli[26], M. Yurko[18], W. Zeuner[8], G.T. Zorn[17].

[1]School of Physics and Space Research, University of Birmingham, Birmingham B15 2TT, UK
[2]Dipartimento di Fisica dell' Università di Bologna and INFN, I-40126 Bologna, Italy
[3]Physikalisches Institut, Universität Bonn, D-53115 Bonn, Germany
[4]Department of Physics, University of California, Riverside CA 92521, USA
[5]Cavendish Laboratory, Cambridge CB3 0HE, UK
[6]Carleton University, Department of Physics, Colonel By Drive, Ottawa, Ontario K1S 5B6, Canada
[7]Centre for Research in Particle Physics, Carleton University, Ottawa, Ontario K1S 5B6, Canada
[8]CERN, European Organisation for Particle Physics, CH-1211 Geneva 23, Switzerland
[9]Enrico Fermi Institute and Department of Physics, University of Chicago, Chicago IL 60637, USA
[10]Fakultät für Physik, Albert Ludwigs Universität, D-79104 Freiburg, Germany
[11]Physikalisches Institut, Universität Heidelberg, D-69120 Heidelberg, Germany
[12]Indiana University, Department of Physics, Swain Hall West 117, Bloomington IN 47405, USA
[13]Queen Mary and Westfield College, University of London, London E1 4NS, UK
[14]Birkbeck College, London WC1E 7HV, UK
[15]University College London, London WC1E 6BT, UK
[16]Department of Physics, Schuster Laboratory, The University, Manchester M13 9PL, UK
[17]Department of Physics, University of Maryland, College Park, MD 20742, USA
[18]Laboratoire de Physique Nucléaire, Université de Montréal, Montréal, Quebec H3C 3J7, Canada
[19]University of Oregon, Department of Physics, Eugene OR 97403, USA
[20]Rutherford Appleton Laboratory, Chilton, Didcot, Oxfordshire OX11 0QX, UK
[21]DAPNIA/SPP, Saclay, F-91191 Gif-sur-Yvette, France
[22]Department of Physics, Technion-Israel Institute of Technology, Haifa 32000, Israel
[23]Department of Physics and Astronomy, Tel Aviv University, Tel Aviv 69978, Israel
[24]International Centre for Elementary Particle Physics and Department of Physics, University of Tokyo, Tokyo 113, and Kobe University, Kobe 657, Japan
[25]Brunel University, Uxbridge, Middlesex UB8 3PH, UK
[26]Particle Physics Department, Weizmann Institute of Science, Rehovot 76100, Israel
[27]Universität Hamburg/DESY, II Institut für Experimental Physik, Notkestrasse 85, D-22607 Hamburg, Germany
[28]University of Victoria, Department of Physics, P O Box 3055, Victoria BC V8W 3P6, Canada
[29]University of British Columbia, Department of Physics, Vancouver BC V6T 1Z1, Canada
[30]University of Alberta, Department of Physics, Edmonton AB T6G 2J1, Canada
[31]Duke University, Dept of Physics, Durham, NC 27708-0305, USA
[32]Universität Aachen, III Physikalisches Institut, Sommerfeldstrasse 26-28, D-52056 Aachen, Germany

[a]Also at TRIUMF, Vancouver, Canada V6T 2A3

1 Introduction

Within the framework of perturbative Quantum Chromodynamics (QCD), the probability for an energetic gluon or quark to radiate a soft gluon is given by their colour charges, $C_{\rm A} = 3$ and $C_{\rm F} = \frac{4}{3}$, respectively. The consequent differences in properties predicted for jets originating from energetic gluons and quarks have been studied in considerable detail, both theoretically [1]–[5] and experimentally [6]–[9].

In high energy $\rm e^+e^-$ collisions one expects three-jet final states to consist of two quark jets and one gluon jet, and two-jet final states to consist of two quark jets. Simple colour counting arguments [3] predict that at asymptotically high energies the multiplicity ratio of radiated gluons in $q\bar{q}g$ final states relative to $q\bar{q}$ final states is

$$\frac{2C_{\rm F} + C_{\rm A}}{2C_{\rm F}} = \frac{17}{8}. \tag{1}$$

The observed ratio of hadron multiplicities in three- and two-jet final states may be compared with this naïve prediction[1] either by invoking the simple hypothesis of local parton-hadron duality (LPHD) [10], in which the hadron flow follows the parton flow, or by using a hadronisation model to describe the conversion of partons into hadrons. Previous experimental measurements have concentrated on comparing the properties of enriched samples of gluon and quark jets, and the existence of different particle multiplicities within these two types of jets was confirmed, in a model independent analysis, in a recent OPAL study [9]. Rather than studying gluon and quark jets directly, the present analysis will instead compare the multiplicity of three-jet events with that of two-jet events.

A recent theoretical paper [1] proposed comparing two- and three-jet exclusive final states by using the $k_\perp$ jet clustering algorithm [11] to define a "sub-jet" or "cluster" multiplicity to replace the simple hadron multiplicity. From a theoretical point of view, using such a sub-jet multiplicity has the advantage that the quantity being calculated is both infra-red and colinear safe and so it can be calculated to all orders in perturbation theory (for large leading and next-to-leading logarithms). Furthermore, the predictions are normalised absolutely, in contrast to predictions of hadron multiplicity which invariably include an arbitrary normalisation parameter. From the experimental side, studying sub-jet multiplicity has advantages similar to analysing jet production rates, *viz.* the effects of hadronisation can be small, it is relatively insensitive to variation of experimental cuts and the procedure can be easily applied to the data.

These calculations predict large corrections, relative to the naïve prediction of Equation 1, which are due to interference effects related to the coherent branching of soft gluons. The sub-jet multiplicity technique is used here to analyse multihadronic decays of the $\rm Z^0$ and the data are compared with both the QCD calculations of [1], and also with various coherent and incoherent QCD Monte Carlo models. This study complements earlier OPAL studies on coherence effects, in particular [12]. The sub-jet analysis technique has also been investigated briefly in an earlier study [13].

[1] The actual hadron multiplicity in the final state is neither colinear nor infra-red safe and is not directly calculable in perturbative QCD.

This paper is organised in the following way: Section 2 contains a brief overview of the OPAL detector and the data selection procedure, Section 3 describes the sub-jet multiplicity observables, Section 4 reviews the correction procedure applied to the data, Section 5 presents the experimental data and compares them with the calculations of [1] and also with various Monte Carlo models, and Section 6 describes the study of systematic uncertainties. Finally, Section 7 summarises the results and draws conclusions regarding their implication for the existence of coherence effects in the data.

2 The OPAL detector and data selection

A detailed description of the OPAL detector has been presented elsewhere [14] and therefore only the features relevant to this analysis are summarised here.

Charged particle trajectories are reconstructed using the cylindrical central tracking detectors, which for the purpose of this analysis consist of a high precision vertex detector, a large volume jet chamber and thin z-chambers. The vertex detector, approximately 100 cm in length and 24 cm in radius, has a spatial resolution of about 50 μm in the r-ϕ plane[2]. This is surrounded by the jet chamber, about 400 cm in length and 185 cm in radius, which provides up to 159 space points per track. The z-chambers, which improve considerably the measurement of charged tracks in θ, are situated immediately beyond and co-axial with the jet chamber. The entire central detector is contained within a solenoid which provides an axial magnetic field of 0.435 T. The track finding is nearly 100% efficient within the angular region $|\cos\theta| < 0.97$.

The electromagnetic calorimeter measures the energy of electrons and photons as well as making a partial energy measurement for hadrons. It consists of a cylindrical ensemble of 9440 lead glass blocks arranged such that the inter-block gaps point slightly away from the origin, and of two end caps, each having 1132 lead glass blocks aligned parallel to the beam axis. The barrel encompasses the angular region $|\cos\theta| < 0.82$ whilst the end caps cover the region $0.81 < |\cos\theta| < 0.98$. The calorimeter has an average depth of around 25 radiation lengths with each individual block subtending a solid angle of approximately 40×40 mrad^2 at the origin, giving an overall coverage of 98% of 4π.

The basic entities used in the analysis were charged tracks and clusters of electromagnetic energy. Charged tracks were required to have at least 40 hits in the jet chamber, a momentum component in the plane perpendicular to the beam axis of greater than 0.15 GeV/c, and a measured momentum of less than 60 GeV/c. The extrapolated point of closest approach of each track to the interaction point was required to be less than 2 cm in the r-ϕ plane and less than 25 cm in z. Clusters in the electromagnetic calorimeter were required to have a measured energy greater than 0.1 GeV if they occurred in the barrel region of the detector, whilst those occurring in the endcap region were required to have a measured energy greater than 0.2 GeV and to consist of at least two lead glass blocks. Blocks which had been observed to be noisy were excluded from the analysis. An electromagnetic cluster was classed as being associated to a charged track if, after the track had been extrapolated to the front face of the

[2]The OPAL coordinate system is defined such that the origin is at the geometric centre of the jet chamber, z is parallel to, and has positive sense along, the e^- beam direction; r is the coordinate normal to z, θ is the polar angle with respect to $+z$ and ϕ is the azimuthal angle around z.

calorimeter, the match in position was better than 150 mrad in θ and 80 mrad in ϕ for clusters in the barrel region, or better than 50 mrad in both θ and ϕ for clusters in the endcap region. The energy of charged particles and neutral clusters was evaluated assuming pion and photon masses, respectively.

Due to its high level of redundancy and fine detector segmentation, the efficiency of the OPAL trigger system [15] for selecting multihadronic events has been estimated to be essentially 100%. Similarly, both the online event filter [16] and the offline selection criteria [17] are extremely efficient. In order to ensure that all events were well contained within the active volume of the detector and to remove residual background, a few additional requirements were imposed on the data sample. The components of the detector and trigger which were used for this analysis were required to be fully operational and only events which were accumulated at centre of mass energies within 0.25 GeV of 91.2 GeV were studied. Events were required to contain at least five charged tracks to reject $\tau^+\tau^-$ final states. Finally, to reject events in which a significant number of particles may have been outside the acceptance of the detector (very close to the beam axis), the thrust axis [18], calculated using all charged tracks and all clusters of electromagnetic energy, was required to have a polar angle $\theta_{\rm thrust}$ which satisfied $|\cos\theta_{\rm thrust}| < 0.9$.

Monte Carlo studies show that within the angular acceptance of the analysis, defined by the above restriction on $\theta_{\rm thrust}$, these criteria are more than $(99.74 \pm 0.01)\%$ efficient for selecting multihadronic decays of the Z^0. The data sample used was that collected during 1990 and 1991, and after all the above cuts, consisted of 333 846 events.

3 Sub-jet multiplicities

Two- and three-jet event samples are selected using the $k_\perp$ jet clustering algorithm [11]. In this scheme, a jet resolution variable, y_{ij}, is defined for every pair of particles i and j in an event by:

$$y_{ij} = \frac{2\min(E_i^2, E_j^2)(1-\cos\theta_{ij})}{E_{\rm vis}^2} \quad , \tag{2}$$

where E_i and E_j are the energies of particles i and j, θ_{ij} is the angle between them and $E_{\rm vis}$ is the sum of all particle energies in the event. If the smallest value of y_{ij} in an event is less than some resolution scale $y_{\rm cut}$, then the particles i and j are merged, being replaced by the sum of their four-momenta. The process is repeated, with the jet resolutions being re-evaluated in each iteration, until all pairs i and j satisfy $y_{ij} > y_{\rm cut}$. Each four-momentum vector which remains at the end of this process is referred to as a "jet". With this algorithm, the minimum transverse momentum between two jets, resolved at a scale defined by $y_{\rm cut}$, is approximately given by:

$$k_\perp^{\rm min} \approx E_{\rm vis}\sqrt{y_{\rm cut}} \quad . \tag{3}$$

In this analysis, the selection of two- and three-jet events is carried out at a jet resolution scale y_1, where $y_1 \sim \mathcal{O}(10^{-2})$. The same jet clustering algorithm is then reapplied to the sample of three-jet events using a variety of resolution scales, $y_0 < y_1$. The mean multiplicity of "sub-jets" or "clusters" found in this way, M_3, as a function of the sub-jet resolution scale,

y_0, is an observable for which resummed QCD calculations exist [1]. As the sub-jet multiplicity is measured using the $k_\perp$ jet finding algorithm, hadronisation effects are expected to be small [11]. Experimental systematic effects are found to be small, as discussed later. The same procedure is carried out using the sample of two-jet events to determine the analogous mean sub-jet multiplicity, M_2, for which calculations are also given in [1].

In the selection of jets described above, particles are defined to be charged tracks and unassociated electromagnetic clusters. To reduce the effect of detector acceptance on the sub-jet multiplicity measured, an event is rejected if any of the two or three jets selected at the scale y_1 has a polar angle $\theta_{\rm jet}$ which does not satisfy $|\cos\theta_{\rm jet}| < 0.9$. This criterion rejects approximately 30 000 additional hadronic events. Throughout the analysis, no restrictions are imposed upon either the number of constituent particles or the energy of each sub-jet, which allows the sub-jet multiplicity to be studied at very small resolution scales, $y_0 \sim \mathcal{O}(10^{-5})$. (The smallest scale considered in this analysis is $y_0 = 6 \cdot 10^{-6}$, which corresponds to a minimum transverse momentum between two jets of approximately 0.18 GeV.)

An attractive feature of this technique is that it is possible to compare experimentally observed sub-jet multiplicities in two- and three-jet events with those calculated in perturbative QCD. By invoking the hypothesis of local parton-hadron duality, the observables M_2 and M_3 are assumed to correspond to the parton jet multiplicities in $q\bar{q}$ and $q\bar{q}g$ events, respectively, where the latter contain a single resolved gluon at the scale y_1. By forming the ratio of the sub-jet multiplicities for three- and two-jet samples, M_3/M_2, further systematic effects may be expected to cancel, giving a very well behaved observable for comparison with the calculations. At finite LEP energies and sub-jet multiplicities, particularly for $y_0 \sim y_1$, it is also useful to consider the ratio $(M_3-3)/(M_2-2)$, in which the number of initiating jets has been subtracted from each sample. This observable describes the multiplicity of additional sub-jets resolved in three-jet events compared to two-jet events, and is therefore more sensitive for the case of $M_3 \sim 3$, $M_2 \sim 2$, while yielding the same result as in Equation (1) for high multiplicities.

At very small values of the sub-jet resolution parameter, $y_0 \sim \mathcal{O}(10^{-5})$, the sub-jet multiplicity tends towards (and at sufficiently small y_0, equals) the particle multiplicity. While perturbative QCD calculations are only appropriate at scales $y_0 \gg 10^{-5}$ at LEP energies [1], QCD Monte Carlo models, which include a simulation of the non-perturbative hadronisation process, can be compared with the data over the full y_0 domain.

4 Method of data correction

The observables described above were constructed from the OPAL data using charged tracks and unassociated electromagnetic clusters. A detailed Monte Carlo simulation of the OPAL detector [19] was then used to correct the data for the effects of finite experimental resolution and acceptance. In this procedure the data were also corrected to an initial state with a well defined centre of mass energy, by removing the effects of initial state photon radiation. This is a minor correction as only the data collected close to the Z^0 peak energy were analysed. The correction procedure employed a bin-by-bin technique. For the reasons discussed above, no hadronisation correction was made, following [20]. In addition, the multiplicity of sub-jets in the data may be considerably greater than the multiplicity of soft gluons generated in the

Monte Carlo models at small y_0, due to cut-offs in the model implementations, making it less appropriate to apply such a correction.

Two Monte Carlo samples were used: a sample (I) with no initial state photon radiation and no detector simulation, and a sample (II), generated using the same Monte Carlo model but including detector simulation and initial state radiation. The QCD parton shower model JETSET [21], version 7.3, with parameters tuned to OPAL data on global event shapes [22], was used to derive the default correction factors. The events of sample (I) consist of all stable charged and neutral particles (those with mean lifetimes greater than $3 \cdot 10^{-10}$ s), including neutrinos. The events of sample (II) were processed by the same reconstruction programs and subjected to the same event selection criteria as the OPAL data.

Defining $\mathcal{H}_i$ to be the value of the observable which is being investigated (*e.g.* the sub-jet multiplicity ratio, M_3/M_2) in bin i of a distribution for sample (I), and $\mathcal{D}_i$ to be the corresponding quantity for the events which remain after event reconstruction and selection, in sample (II), the correction factor $\mathcal{C}_i$ for bin i is then given by $\mathcal{C}_i = \mathcal{H}_i/\mathcal{D}_i$. The experimental measurement, for bin i of the distribution in question, is corrected by multiplying it by the factor $\mathcal{C}_i$. As this correction only accounts for effects of measurement with the OPAL detector and initial state radiation, the data are said to be corrected to the *hadron level*. Further details of the correction procedure and the estimation of the associated uncertainties are given in Section 6; the correction factors for each of the observables M_3 and M_2 represent at most a 7.5% correction, whilst the corresponding correction for the ratios of observables is 2.5%.

5 Results

Distributions of the various sub-jet multiplicity observables, namely M_3, M_2, M_3/M_2 and $(M_3-3)/(M_2-2)$ as functions of y_0, were constructed using the data and then corrected to the hadron level. These observables were studied for four different values of the jet selection scale y_1, in the interval $0.007 < y_1 < 0.023$; one of these is $y_1 = 0.01$ for which the calculations of [1] were performed. As jet multiplicity is found to have an approximately logarithmic dependence upon the resolution parameter, y_1 values are chosen such that each is a constant factor of roughly 1.5 larger than the previous value. The corrected data are then compared with theoretical predictions in the form of both analytic perturbative QCD calculations and also of QCD Monte Carlo models, as described below. The values of these observables, for each of the four y_1 values chosen, are given in Tables 1–4, where the errors include the statistical error on the data and on the correction factors, added in quadrature to the systematic error, the estimation of which is discussed in Section 6. The figures presented below contain approximately 300 000 multihadronic events. It should be noted that all events selected at the scale y_1 contribute at each value of y_0, and so successive bins in each distribution are correlated.

5.1 Comparison with analytic QCD calculations

The distribution of M_3/M_2 observed in the data for $y_1 = 0.01$ is shown in Figure 1, where the error given on each point includes (and is dominated by) systematic uncertainties. By

construction, this distribution has a value of 1.5 at $y_0 = y_1$, the resolution scale at which the initial two- and three-jet events are selected. It is seen to fall off with decreasing y_0 and remains far below the naïve expectation of 17/8 given in Equation (1) over the entire range considered.

The figure also shows the predictions of [1]; a calculation in which the leading and next-to-leading logarithmic terms are evaluated to fixed order in α_s, and also an involved calculation in which leading and next-to-leading logarithmic terms are evaluated to all orders in α_s (NLLA calculation). The fixed order calculation includes final states with up to four partons and therefore the description of the gluon radiation consists of logarithmic terms to order α_s^2 for the $q\bar{q}$ initial state and to order α_s for the $q\bar{q}g$ case. It is useful to show both calculations to demonstrate the change in behaviour of the QCD prediction when higher order terms are included in the calculation. The moderate variation in the NLLA calculation for different choices of the effective QCD scale, Λ, is shown. The present calculations are not sufficiently complete for this Λ to correspond to $\Lambda_{\overline{MS}}$; however, it is expected to be of a comparable magnitude, *i.e.* $\Lambda \sim 0.20$ GeV. The calculations are carried out to some value of y_0, below which non-perturbative considerations are expected to be significant; this lower bound is a function of the particular Λ chosen. Both fixed order and all orders calculations exhibit qualitatively similar behaviour to the data for y_0 close to y_1 and an appropriate choice of Λ, but disagree for smaller y_0 values where the calculations predict M_3/M_2 to increase with decreasing y_0. This rise is appreciably suppressed in the NLLA calculation compared to the fixed order one, thus improving the description of the data, particularly at higher values of y_0. The solid curve depicts the behaviour of the NLLA calculation for $\Lambda = 0.35$ GeV, which is chosen for use in the following comparisons.

The fall of M_3/M_2 is attributed in [1] to coherence of soft gluon radiation. The three-jet sample selected at small values of y_1 is likely to contain events in which a hard gluon has been radiated at a relatively small angle, θ_g, with respect to its parent quark. Subsequent gluon emission by this resolved, hard gluon is restricted on average by destructive interference effects to be within the initial emission angle θ_g ("angular ordering"), resulting in a lowering of the effective colour charge of the gluon initiated jet. It is shown in [1] that this reduction is such that the effective colour charge of the gluon jet is less than that of a quark jet, leading to M_3/M_2 having a value smaller than 1.5, as observed in the data.

At larger jet selection scales, y_1, the three-jet sample is likely to contain fewer events with small θ_g, and the suppression of the effective colour charge of the gluon jet due to coherence effects is expected to be reduced. This is, in turn, expected to cause a decrease in the slope of M_3/M_2 at $y_0 = y_1$, for larger y_1. This trend is observed in the data; it is seen from the variation of the slope, which can be determined using the last measured y_0 point, for each of the four y_1 values given in Table 1.

The sub-jet multiplicity for three-jet events observed in the OPAL data is shown in Figure 2, for two different values of the jet selection scale, y_1. The distribution presented is in the form $M_3 - 3$, *i.e.* the initial number of jets in the sample has been subtracted from the corrected mean sub-jet multiplicity, M_3, leaving only the additional number of sub-jets resolved as a function of y_0. At very small values of y_0, M_3 itself tends towards the hadron level multiplicity, while at $y_0 = y_1$, $M_3 - 3$ is constrained to be zero. The mean particle multiplicity at $y_1 = 0.007$, corrected to the hadron level, is measured to be approximately 45 for three-jet events whilst that for two-jet events is found to be 35. Also given in this figure are the predictions of the two

calculations described above. There is fairly good qualitative description of the data by the NLLA calculations over the entire range of their validity, whereas the fixed order calculations give a significantly poorer description, particularly for $y_0 \lesssim 10^{-3}$. The analogous distributions for events having two resolved jets at $y_0 = y_1$, *i.e.* $M_2 - 2$ as a function of y_0, are given in Figure 3, along with the corresponding QCD predictions. Similarly, a fairly good qualitative agreement is found between the data and the NLLA calculations, and a somewhat worse agreement is found for the fixed order calculations.

The ratio of the sub-jet multiplicities after subtraction of the number of initial jets in each sample, *i.e.* $(M_3 - 3)/(M_2 - 2)$, is illustrated in Figure 4. This observable is undefined for $y_0 = y_1$, and then increases rapidly with decreasing y_0, down to a resolution scale $y_0 \sim 4 \cdot 10^{-4}$, below which it is seen to flatten off. This value of y_0 is equivalent to a minimum transverse momentum between two resolved sub-jets of approximately 1.8 GeV, using Equation (3) with $E_{\rm vis} = 91.2$ GeV. Above this y_0, in the region of rapid rise, the rate at which sub-jets are resolved in the three-jet sample as a function of decreasing y_0 is greater than that for the two-jet sample. Identifying the sub-jets with soft gluons in an event, the interpretation of this is that perturbative effects are being observed; the rate of resolving radiated soft gluons as a function of decreasing y_0 is higher in a three-jet event than that for a two-jet event, for gluons with a minimum transverse momentum (with respect to the radiating parton) of at least 1.8 GeV. Below this y_0, the rate of resolving sub-jets within the three- and two-jet samples is essentially the same. This might be reasonable behaviour for the data, if these sub-jets are only probing the hadronisation products of soft gluons produced in the perturbative region and soft gluons produced from a quark initiated jet hadronise in the same way as those from a gluon jet. These regions are referred to as perturbative and non-perturbative hereafter.

Figure 4 also shows results of the analytic calculations. The NLLA calculations are seen to give a good qualitative description of the data, and are in excellent quantitative agreement for $y_1 = 0.007$, in the perturbative region. This perturbative region is defined according to the data, as described above, rather than by the lowest y_0 for which the calculations are deemed quantitatively reliable. By varying Λ, the calculations can describe data at both values of y_1 equally well, but a single value of Λ does not accommodate both distributions simultaneously.

Following the observation of the decrease in the slope of M_3/M_2 with increasing y_1 discussed above, it is also seen from the data in Table 4 that at any given y_0 scale, the value of $(M_3 - 3)/(M_2 - 2)$ increases with increasing y_1. This is postulated to follow from a lowering in the suppression of the effective colour charge of gluon jets with increasing y_1, which is a consequence of the increased $\theta_{\rm g}$ of gluon jets in the three-jet sample.

5.2 Comparison with QCD Monte Carlo models

The data are compared with various QCD Monte Carlo models, in a similar manner to the above comparisons with analytic QCD predictions. Distributions of $M_3 - 3$ and $M_2 - 2$ are shown for two different values of the scale y_1 and $(M_3 - 3)/(M_2 - 2)$ is presented for four values of y_1. The ratio M_3/M_2, although studied, is not shown, as $(M_3 - 3)/(M_2 - 2)$ offers a greater discrimination between models, and the data themselves have already been shown for M_3/M_2. For each observable, one of the y_1 values used is $y_1 = 0.01$, as this was also used in comparing

data with calculations. The largest value used is $y_1 = 0.023$, which was considered too high to be used in the previous set of comparisons, because the NLLA calculation is quantitatively less reliable for small $\ln(1/y_1)$.

The Monte Carlo models discussed below are the following:

- The JETSET model, version 7.3 [21], using a coherent parton shower and Lund symmetric (string) fragmentation. The parameters used were tuned to OPAL data on global event shapes [22].
- The HERWIG program, version 5.5 [23], with coherent parton shower and cluster fragmentation. The parameters used were based upon a tuning to OPAL data on global event shapes [9].
- The ARIADNE model, version 3.1 [24], with a colour dipole formulation of the coherent parton shower, and the standard Lund string fragmentation model [25]. The parameters were tuned to OPAL data, as described in [22].
- The COJETS model, versions 6.23 and 6.12 [26], with an incoherent parton shower and independent fragmentation. The parameters of the model were tuned by its authors to fit OPAL data on event shapes [27]. It should be noted that in version 6.23 of the program, different fragmentation parameters are used for quarks and gluons, whereas this is not the case in version 6.12.

Figure 5 shows the sub-jet multiplicity for three-jet events in the form $M_3 - 3$, as discussed earlier for Figure 2. The models give a fairly good quantitative description of the data: the value of $M_3 - 3$ predicted by a given model was found to be within 10% of that observed in the data for all y_0 considered, except for COJETS versions 6.23 and 6.12 where this difference was in the range 15–20%. Furthermore, a wider variation is seen between the predictions of the different models for $y_0 \sim y_1$ at large y_1. Similarly, Figure 6 shows the sub-jet multiplicity for two-jet events in the form $M_2 - 2$, following Figure 3. As in the three-jet case, all models provide a good description of the data, with differences from the data of less than approximately 10%; ARIADNE , HERWIG and JETSET have essentially a constant difference from the data for all y_0, whereas the COJETS models exhibit a non-uniform difference across the y_0 range. From these distributions, it is seen that the models describe the two-jet data slightly better than the three-jet data in the high y_0 region. It is also seen in both the three- and two-jet cases that the predictions of the models are systematically about 5% higher than the values observed in the data.

The next set of distributions studied is the ratio $(M_3 - 3)/(M_2 - 2)$, shown in Figures 7 and 8, where the behaviour of the data themselves was previously described in Section 5.1. This observable provides a good test of the models, when considered in addition to the comparisons of $M_3 - 3$ and $M_2 - 2$ with data given above, as it combines their ability to describe the behaviour of the data for both three- and two-jet cases simultaneously. It can be seen that most models describe the general form of the data. Considering all four y_1 values, the COJETS model, version 6.23, gives the poorest overall description of the data, whilst both versions of this model give the least accurate description of the data in the perturbative region. The ARIADNE model is found to give the best overall description of the data in the perturbative

region; JETSET tends to underestimate the data in the perturbative region at all but the smallest y_1 considered, but gives the best description in the non-perturbative region. (This remains the case even after the parameters Λ, Q_0, σ_q and a of the JETSET model were each varied independently by the uncertainties given in [22].) HERWIG predicts a rather less distinct flattening off in the non-perturbative region, for all y_1, than is seen in the data.

The final comparison with Monte Carlo models was performed using the JETSET program, which allows both the parton shower and the fragmentation scheme to be changed in a convenient manner. The models used were all tuned to OPAL event shape data in essentially the same way, and consisted of:

(a) Coherent parton shower and string fragmentation, with parameters from [22], as used in the earlier model comparisons.

(b) Coherent parton shower and independent fragmentation, with parameters as given in Table 5.

(c) Incoherent parton shower and string fragmentation, with parameters from [12].

(d) Incoherent parton shower and independent fragmentation, with parameters as given in Table 5.

(e) Coherent parton shower and the fragmentation model of Peterson *et al.* [28] for heavy (b and c) quarks, with parameters from [9], and Lund string fragmentation for light quarks.

The result of this study is shown in Figure 9, for $y_1 = 0.01$. As was seen in Figure 7, the default JETSET model, labelled (a) above, tends to underestimate the data slightly in the perturbative region. The effect of using the Peterson fragmentation scheme for heavy quark flavours seems to be small, whereas using independent fragmentation leads to a significantly poorer agreement when using a coherent parton shower. The two models with an incoherent parton shower predict a considerably higher value for the observable than is seen in the data. It is interesting to compare the difference between the two models which have an incoherent parton shower with the difference between the corresponding models which have a coherent parton shower; the effect of independent fragmentation seems to be to increase the observed value across much of the y_0 range, irrespective of the type of parton shower employed. The model with an incoherent parton shower and independent fragmentation in this figure is also seen to behave in a very similar manner to the COJETS model, version 6.23, given in Figure 7.

6 Estimation of systematic uncertainties

Systematic uncertainties have been studied as summarised below. The most significant source of systematic uncertainty arises from correcting the observed data to the hadron level. To estimate the uncertainty associated with this procedure, each observable was measured in the data using four different definitions for observed particles, while retaining the same event selection criteria as described in Section 2. The definitions of particles used were: charged tracks and

unassociated clusters of electromagnetic energy, charged tracks alone, clusters of electromagnetic energy alone, and charged tracks and all clusters of electromagnetic energy. The same distributions were constructed using the simulated OPAL data, allowing the data to be corrected to the hadron level in four different ways. One half of the largest difference between any of the four corrected distributions in each bin was taken to be the systematic uncertainty arising from the correction procedure. This analysis was carried out for all observables at all four values of y_1. The uncertainty was found to be in the range from 0.6% for M_3/M_2 up to approximately 3% for $(M_3-3)/(M_2-2)$. The correction factors themselves represent at most a 2.5% correction for both ratios of the sub-jet multiplicity studied, whilst the corresponding correction may be as large as 7.5% for the constituent M_3 and M_2 distributions.

The effect of tightening the restriction on the polar angle, $\theta_{\rm jet}$, of each jet selected at $y_0 = y_1$, from $|\cos\theta_{\rm jet}| < 0.9$ to $|\cos\theta_{\rm jet}| < 0.7$ was studied. No statistically significant effect was found. The effect of removing the restriction on $\theta_{\rm jet}$ and also of varying the definition of particles used to calculate the thrust axis, as described above, was found to be negligible. The insensitivity of the data to these cuts was also substantiated in a study using hadrons generated with the JETSET Monte Carlo to provide an approximate modelling of experimental cuts, without using a full detector simulation; for example, the effect of applying fiducial cuts on the particle acceptance, the polar angle of the jets and on the polar angle of the thrust axis was found to produce a variation of no more than 0.25% in the value of M_3/M_2. No statistically significant effects were seen when small variations were made to the experimental definition of charged tracks and clusters of electromagnetic energy used in the analysis. The data were divided into ten subsets containing approximately equal numbers of events and analysed separately; consistent results were found in all cases. In order to test further the sensitivity to the definition of particles used in the analysis, two- and three-jet events were selected using charged tracks and all clusters of electromagnetic energy and the remainder of the analysis was performed with the definition that particles were charged tracks and unassociated electromagnetic clusters. Again, no statistically significant difference was seen as a result of this test.

The central value given in all tables and figures is evaluated by correcting the data to the hadron level using the JETSET model, version 7.3, with a coherent parton shower and string fragmentation. The data were also corrected to the hadron level using three other Monte Carlo models, namely the JETSET model with a coherent parton shower and Peterson fragmentation for heavy quark flavours, the HERWIG program and version 6.23 of the COJETS model. The tuning of parameters for each of these models is the same as was used above. For each observable, one half of the largest difference between any of the four corrected distributions in each bin was taken to be the systematic uncertainty arising from the model dependence of the correction procedure. This study was performed at all values of y_1 considered in the analysis. The additional systematic uncertainties assigned were at most 1.0% for M_3, 1.3% for M_2, 0.5% for M_3/M_2 and 3.5% for $(M_3-3)/(M_2-2)$. These were added in quadrature to the systematic uncertainties estimated above, associated with detector corrections due to the definition of particles.

7 Discussion and summary

The sub-jet multiplicities have been measured in the OPAL detector and compared with analytic perturbative QCD calculations, based upon the summation of leading and next-to-leading logarithms to all orders in α_s, as well as with QCD Monte Carlo models. The NLLA calculations give a fairly good qualitative description of the number of additional sub-jets resolved in both three-jet events and two-jet events. The ratio $(M_3 - 3)/(M_2 - 2)$ shows two distinct regions, which may be associated with the dominance of perturbative and non-perturbative effects in the data; defining the perturbative region in this way, the NLLA calculations are in quantitative agreement with the data. In this perturbative region, the measured distribution of M_3/M_2 is described qualitatively by the NLLA calculations, supporting the validity of the large corrections predicted (relative to the result of Equation 1) due to interference effects related to soft gluon emission. The variation of the slope of M_3/M_2 near to the sub-jet production threshold as a function of y_1, and similarly the increase in the resolved sub-jet multiplicity in three-jet events relative to two-jet events for increasing y_1, are in agreement with the expectation based on coherence of soft gluon radiation.

Most Monte Carlo models considered are found to give a good quantitative description of the data, with a slightly smaller variation in the prediction between models and also a better agreement with the data in the two-jet case than in the three-jet case. The diversity of the predictions for the three-jet case is seen to be greater for $y_0 \sim y_1$ for larger y_1. Although a good general agreement was found between the various models and the data for the ratio $(M_3 - 3)/(M_2 - 2)$, significant differences were seen. The models ARIADNE and JETSET provide the best overall description of the data in the perturbative and non-perturbative regions, respectively. The COJETS models give the least accurate predictions, version 6.23 being the poorest in this respect. A study of different fragmentation and parton shower schemes using the JETSET model bears out the observation made for the COJETS models, showing that the incoherent models considered have serious discrepancies with the data in both the perturbative and non-perturbative regions. The fact that the data are well described by analytic perturbative QCD calculations, and that Monte Carlo models with a coherent parton shower provide a significantly better description of the data than models with an incoherent parton shower, suggests that coherence effects are present in the observed data, supporting the conclusions of [12].

Acknowledgements

We thank B.R. Webber for providing computer code to perform the all orders calculation described in [1] and also for comments on the text.

It is a pleasure to thank the SL Division for the efficient operation of the LEP accelerator, the precise information on the absolute energy, and their continuing close cooperation with our experimental group. In addition to the support staff at our own institutions we are pleased to acknowledge the
Department of Energy, USA,
National Science Foundation, USA,
Texas National Research Laboratory Commission, USA,
Science and Engineering Research Council, UK,
Natural Sciences and Engineering Research Council, Canada,
Fussefeld Foundation,
Israeli Ministry of Energy and Ministry of Science,
Minerva Gesellschaft,
Japanese Ministry of Education, Science and Culture (the Monbusho) and a grant under the Monbusho International Science Research Program,
German Israeli Bi-national Science Foundation (GIF),
Direction des Sciences de la Matière du Commissariat à l'Energie Atomique, France,
Bundesministerium für Forschung und Technologie, Germany,
National Research Council of Canada,
A.P. Sloan Foundation and Junta Nacional de Investigação Científica e Tecnológica, Portugal.

References

[1] S. Catani, Yu.L. Dokshitzer and F. Fiorani, B.R. Webber, Nucl. Phys. **B383** (1992) 419.

[2] S. Catani, Yu.L. Dokshitzer and F. Fiorani, B.R. Webber, Nucl. Phys. **B377** (1992) 445;

[3] S.J. Brodsky and J. Gunion, Phys. Rev. Lett. **37** (1976) 402;
K. Konishi, A. Ukawa and G. Veneziano, Phys. Lett. **B78** (1978) 243.

[4] K. Shizuya and S.-H.H. Tye, Phys. Rev. Lett. **41** (1978) 787;
M.B. Einhorn and B.G. Weeks, Nucl. Phys. **B146** (1978) 445;
H.P. Nilles and K.H. Streng, Phys. Rev. **D23** (1981) 1944;
A.H. Mueller, Nucl. Phys. **B241** (1984) 141;
J.B. Gaffney and A.H. Mueller, Nucl. Phys. **B250** (1985) 109.

[5] Yu.L. Dokshitzer, V.A. Khoze and S.I. Troyan,
Perturbative Quantum Chromodynamics, ed. A. Mueller (World Scientific, Singapore) 1989;
Yu.L. Dokshitzer, V.A. Khoze, A.H. Mueller and S.I. Troyan,
Basics of Perturbative QCD (Editions Frontières, Paris) 1991.

[6] DELPHI Collaboration, P. Abreu *et al.*, Z. Phys. **C56** (1992) 63.

[7] JADE Collaboration, W. Bartel *et al.*, Phys. Lett. **123B** (1983) 460;
UA2 Collaboration, P. Bagnaia *et al.*, Phys. Lett. **144B** (1984) 291;
HRS Collaboration, M. Derrick *et al.*, Phys. Lett. **165B** (1985) 449;
MARK2 Collaboration, A. Petersen *et al.*, Phys. Rev. Lett. **55** (1985) 1954;
UA1 Collaboration, G. Arnison *et al.*, Nucl. Phys. **B276** (1986) 253;
TASSO Collaboration, W. Braunschweig *et al.*, Z. Phys. **C45** (1989) 1;
AMY Collaboration, Y.K. Kim *et al.*, Phys. Rev. Lett. **63** (1989) 1772.
CLEO Collaboration, M.S. Alam *et al.*, Phys. Rev. **D46** (1992) 4822.

[8] OPAL Collaboration, G. Alexander *et al.*, Phys. Lett. **B265** (1991) 462.

[9] OPAL Collaboration, P.D. Acton *et al.*, Z. Phys. **C58** (1993) 387.

[10] D. Amati and G. Veneziano, Phys. Lett. **B83** (1979) 87;
Ya.I. Azimov, Yu.L. Dokshitzer, V.A. Khoze and S.I. Troyan, Z. Phys. **C27** (1985) 65.

[11] N. Brown and W.J. Stirling, Phys. Lett. **B252** (1990) 657;
S. Bethke, Z. Kunszt, D. Soper and W.J. Stirling, Nucl. Phys. **B370** (1992) 310;
S. Catani *et al.*, Phys. Lett. **B269** (1991) 432;
N. Brown and W.J. Stirling, Z. Phys. **C53** (1992) 629.

[12] OPAL Collaboration, P.D. Acton *et al.*, Z. Phys. **C58** (1993) 207.

[13] L3 Collaboration, O. Adriani *et al.*, Phys. Rep. **236** (1993) 1.

[14] OPAL Collaboration, K. Ahmet *et al.*, Nucl. Instr. and Meth. **A305** (1991) 275.

[15] M. Arignon *et al.*, Nucl. Instr. and Meth. **A313** (1992) 103.

[16] D.G. Charlton, F. Meijers, T.J. Smith and P.S. Wells, Nucl. Instr. and Meth. **A325** (1993) 129.

[17] OPAL Collaboration, G. Alexander *et al.*, Z. Phys. **C52** (1991) 175.

[18] S. Brandt *et al.*, Phys. Lett. **12** (1964) 57;
E. Farhi, Phys. Rev. Lett. **39** (1977) 1587.

[19] J. Allison *et al.*, Nucl. Instr. and Meth. **A317** (1992) 47.

[20] OPAL Collaboration, M.Z. Akrawy *et al.*, Phys. Lett. **B235** (1990) 389.

[21] T. Sjöstrand, Comp. Phys. Commun. **39** (1986) 347;
T. Sjöstrand, Comp. Phys. Commun. **43** (1987) 367;
M. Bengtsson and T. Sjöstrand, Nucl. Phys. **B289** (1987) 810.

[22] OPAL Collaboration, M.Z. Akrawy *et al.*, Z. Phys. **C47** (1990) 505.

[23] G. Marchesini and B.R. Webber, Nucl. Phys. **B310** (1988) 461;
G. Marchesini *et al.*, Comp. Phys. Commun. **67** (1992) 465.

[24] U. Pettersson, LU TP 88-5 (1988);
L. Lönnblad and U. Pettersson, LU TP 88-15 (1988);
L. Lönnblad, LU TP 89-10 (1988).

[25] B. Andersson, G. Gustafson, G. Ingelman and T. Sjöstrand, Phys. Rep. **97** (1983) 31.

[26] R. Odorico, Comp. Phys. Commun. **32** (1984) 139;
R. Odorico, Comp. Phys. Commun. **59** (1990) 527;

[27] P. Mazzanti and R. Odorico, Nucl. Phys. **B370** (1992) 23.

[28] C. Peterson, D. Schlatter, I. Schmitt and P.M. Zerwas, Phys. Rev. **D27** (1983) 105.

	M_3/M_2			
$\log_{10}(1/y_0)$	$y_1 = 0.007$	$y_1 = 0.010$	$y_1 = 0.015$	$y_1 = 0.023$
5.21	1.258 ± 0.010	1.272 ± 0.008	1.286 ± 0.009	1.299 ± 0.009
5.03	1.259 ± 0.010	1.273 ± 0.009	1.287 ± 0.009	1.299 ± 0.009
4.85	1.262 ± 0.010	1.275 ± 0.009	1.289 ± 0.009	1.301 ± 0.009
4.67	1.265 ± 0.010	1.278 ± 0.009	1.292 ± 0.010	1.304 ± 0.010
4.49	1.271 ± 0.009	1.283 ± 0.009	1.297 ± 0.009	1.309 ± 0.009
4.31	1.276 ± 0.009	1.290 ± 0.008	1.305 ± 0.009	1.315 ± 0.009
4.13	1.285 ± 0.008	1.298 ± 0.008	1.312 ± 0.009	1.323 ± 0.009
3.96	1.293 ± 0.009	1.305 ± 0.008	1.319 ± 0.009	1.329 ± 0.009
3.78	1.304 ± 0.010	1.314 ± 0.009	1.326 ± 0.009	1.338 ± 0.009
3.60	1.317 ± 0.009	1.327 ± 0.008	1.338 ± 0.009	1.348 ± 0.008
3.42	1.330 ± 0.010	1.339 ± 0.008	1.349 ± 0.009	1.358 ± 0.008
3.24	1.342 ± 0.010	1.350 ± 0.009	1.360 ± 0.009	1.370 ± 0.008
3.06	1.355 ± 0.008	1.363 ± 0.008	1.373 ± 0.007	1.381 ± 0.006
2.89	1.372 ± 0.008	1.373 ± 0.008	1.383 ± 0.006	1.390 ± 0.006
2.71	1.397 ± 0.007	1.392 ± 0.008	1.397 ± 0.007	1.402 ± 0.006
2.53	1.426 ± 0.007	1.413 ± 0.007	1.411 ± 0.007	1.411 ± 0.006
2.35	1.461 ± 0.003	1.439 ± 0.006	1.427 ± 0.006	1.421 ± 0.006
2.17	1.5	1.467 ± 0.005	1.446 ± 0.006	1.433 ± 0.006
1.99		1.5	1.470 ± 0.004	1.450 ± 0.005
1.81			1.5	1.473 ± 0.002
1.64				1.5

Table 1: OPAL data, corrected to the hadron level, for M_3/M_2, with combined statistical and systematic uncertainties.

$\log_{10}(1/y_0)$	M_3			
	$y_1 = 0.007$	$y_1 = 0.010$	$y_1 = 0.015$	$y_1 = 0.023$
5.21	20.99 ± 0.38	21.68 ± 0.40	22.37 ± 0.42	22.98 ± 0.43
5.03	19.06 ± 0.32	19.70 ± 0.34	20.32 ± 0.36	20.88 ± 0.37
4.85	17.21 ± 0.28	17.78 ± 0.30	18.34 ± 0.32	18.86 ± 0.32
4.67	15.42 ± 0.25	15.93 ± 0.26	16.44 ± 0.26	16.91 ± 0.27
4.49	13.71 ± 0.22	14.17 ± 0.23	14.63 ± 0.23	15.04 ± 0.24
4.31	12.10 ± 0.19	12.53 ± 0.20	12.94 ± 0.21	13.30 ± 0.21
4.13	10.63 ± 0.17	11.01 ± 0.18	11.39 ± 0.18	11.71 ± 0.18
3.96	9.30 ± 0.14	9.63 ± 0.15	9.96 ± 0.15	10.24 ± 0.16
3.78	8.09 ± 0.12	8.38 ± 0.12	8.67 ± 0.13	8.92 ± 0.13
3.60	7.03 ± 0.10	7.29 ± 0.10	7.54 ± 0.10	7.77 ± 0.11
3.42	6.11 ± 0.08	6.34 ± 0.09	6.56 ± 0.09	6.76 ± 0.09
3.24	5.31 ± 0.06	5.52 ± 0.07	5.72 ± 0.07	5.89 ± 0.07
3.06	4.64 ± 0.05	4.83 ± 0.06	5.00 ± 0.07	5.15 ± 0.07
2.89	4.09 ± 0.05	4.25 ± 0.05	4.41 ± 0.06	4.54 ± 0.06
2.71	3.66 ± 0.04	3.81 ± 0.04	3.94 ± 0.04	4.06 ± 0.04
2.53	3.35 ± 0.02	3.48 ± 0.03	3.60 ± 0.03	3.71 ± 0.03
2.35	3.14 ± 0.01	3.26 ± 0.02	3.37 ± 0.01	3.46 ± 0.02
2.17	3	3.112 ± 0.005	3.21 ± 0.01	3.29 ± 0.01
1.99		3	3.089 ± 0.002	3.159 ± 0.005
1.81			3	3.066 ± 0.003
1.64				3

Table 2: OPAL data, corrected to the hadron level, for M_3, with combined statistical and systematic uncertainties.

	M_2			
$\log_{10}(1/y_0)$	$y_1 = 0.007$	$y_1 = 0.010$	$y_1 = 0.015$	$y_1 = 0.023$
5.21	16.68 ± 0.42	17.05 ± 0.42	17.39 ± 0.43	17.70 ± 0.44
5.03	15.14 ± 0.37	15.48 ± 0.38	15.79 ± 0.38	16.07 ± 0.39
4.85	13.64 ± 0.33	13.95 ± 0.33	14.23 ± 0.34	14.49 ± 0.34
4.67	12.19 ± 0.29	12.47 ± 0.29	12.73 ± 0.30	12.96 ± 0.30
4.49	10.79 ± 0.25	11.04 ± 0.25	11.28 ± 0.26	11.49 ± 0.26
4.31	9.48 ± 0.21	9.71 ± 0.22	9.92 ± 0.22	10.11 ± 0.22
4.13	8.28 ± 0.18	8.49 ± 0.19	8.68 ± 0.19	8.85 ± 0.19
3.96	7.19 ± 0.15	7.38 ± 0.16	7.55 ± 0.16	7.70 ± 0.16
3.78	6.20 ± 0.13	6.38 ± 0.13	6.53 ± 0.14	6.67 ± 0.14
3.60	5.34 ± 0.10	5.50 ± 0.11	5.64 ± 0.11	5.76 ± 0.11
3.42	4.60 ± 0.09	4.74 ± 0.09	4.87 ± 0.09	4.98 ± 0.10
3.24	3.96 ± 0.07	4.09 ± 0.07	4.20 ± 0.08	4.30 ± 0.08
3.06	3.43 ± 0.06	3.54 ± 0.06	3.64 ± 0.06	3.73 ± 0.06
2.89	2.98 ± 0.05	3.09 ± 0.05	3.19 ± 0.05	3.27 ± 0.05
2.71	2.62 ± 0.04	2.73 ± 0.04	2.82 ± 0.04	2.90 ± 0.04
2.53	2.35 ± 0.02	2.46 ± 0.03	2.55 ± 0.03	2.63 ± 0.03
2.35	2.15 ± 0.01	2.27 ± 0.02	2.36 ± 0.02	2.43 ± 0.02
2.17	2	2.12 ± 0.01	2.22 ± 0.01	2.29 ± 0.01
1.99		2	2.10 ± 0.01	2.18 ± 0.01
1.81			2	2.082 ± 0.004
1.64				2

Table 3: OPAL data, corrected to the hadron level, for M_2, with combined statistical and systematic uncertainties.

	$(M_3-3)/(M_2-2)$			
$\log_{10}(1/y_0)$	$y_1 = 0.007$	$y_1 = 0.010$	$y_1 = 0.015$	$y_1 = 0.023$
5.21	1.225 ± 0.011	1.241 ± 0.009	1.258 ± 0.009	1.273 ± 0.009
5.03	1.222 ± 0.011	1.239 ± 0.010	1.256 ± 0.010	1.271 ± 0.010
4.85	1.220 ± 0.011	1.237 ± 0.010	1.254 ± 0.010	1.269 ± 0.010
4.67	1.219 ± 0.011	1.235 ± 0.010	1.253 ± 0.011	1.268 ± 0.011
4.49	1.218 ± 0.010	1.235 ± 0.010	1.253 ± 0.011	1.268 ± 0.010
4.31	1.216 ± 0.010	1.235 ± 0.009	1.255 ± 0.010	1.270 ± 0.009
4.13	1.216 ± 0.010	1.235 ± 0.009	1.256 ± 0.010	1.271 ± 0.010
3.96	1.214 ± 0.010	1.233 ± 0.010	1.253 ± 0.011	1.269 ± 0.010
3.78	1.211 ± 0.012	1.229 ± 0.011	1.250 ± 0.012	1.267 ± 0.011
3.60	1.207 ± 0.011	1.227 ± 0.011	1.249 ± 0.012	1.266 ± 0.010
3.42	1.199 ± 0.015	1.221 ± 0.012	1.243 ± 0.013	1.262 ± 0.012
3.24	1.180 ± 0.015	1.206 ± 0.013	1.232 ± 0.014	1.254 ± 0.012
3.06	1.152 ± 0.014	1.183 ± 0.012	1.215 ± 0.011	1.240 ± 0.010
2.89	1.109 ± 0.018	1.140 ± 0.018	1.182 ± 0.012	1.213 ± 0.011
2.71	1.060 ± 0.022	1.093 ± 0.020	1.138 ± 0.013	1.174 ± 0.013
2.53	0.998 ± 0.028	1.028 ± 0.022	1.075 ± 0.014	1.113 ± 0.017
2.35	0.926 ± 0.030	0.964 ± 0.032	1.003 ± 0.018	1.037 ± 0.020
2.17		0.906 ± 0.044	0.933 ± 0.028	0.957 ± 0.027
1.99			0.863 ± 0.036	0.870 ± 0.026
1.81				0.789 ± 0.029

Table 4: OPAL data, corrected to the hadron level, for $(M_3-3)/(M_2-2)$, with combined statistical and systematic uncertainties.

Model	Parameter	name	Value
Jetset 7.3	Λ (GeV)	PARJ(81)	0.09
coherent parton shower	Q_0 (GeV)	PARJ(82)	1.0
independent fragmentation	σ_q (GeV)	PARJ(21)	0.46
	a	PARJ(41)	0.04
	b (GeV^{-2})	PARJ(42)	0.50
		MSTJ(1)	2
		MSTJ(42)	2
		MSTJ(46)	3
Jetset 7.3	Λ (GeV)	PARJ(81)	0.09
incoherent parton shower	Q_0 (GeV)	PARJ(82)	1.0
independent fragmentation	σ_q (GeV)	PARJ(21)	0.46
	a	PARJ(41)	0.04
	b (GeV^{-2})	PARJ(42)	1.10
		MSTJ(1)	2
		MSTJ(42)	1

Table 5: Monte Carlo parameter values, tuned to OPAL event shape distributions; unlike JETSET models including Lund symmetric fragmentation, these independent fragmentation models do not provide a good description of the data, even after tuning. They are used herein to study the behaviour of different fragmentation schemes.

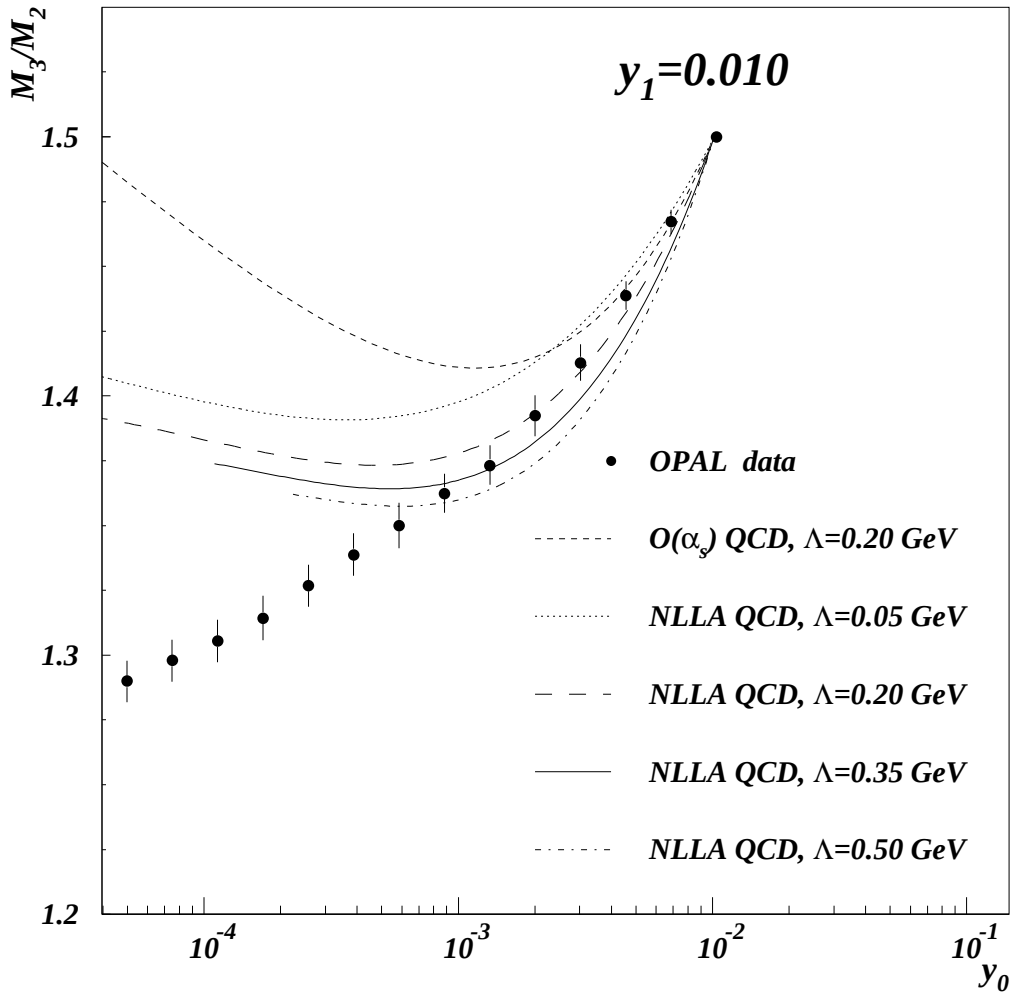

Figure 1: Ratio of sub-jet multiplicity of three-jet and two-jet events. The solid points represent OPAL data (corrected to hadron level), and the analytic QCD calculations for various choices of scale parameter are shown as curves.

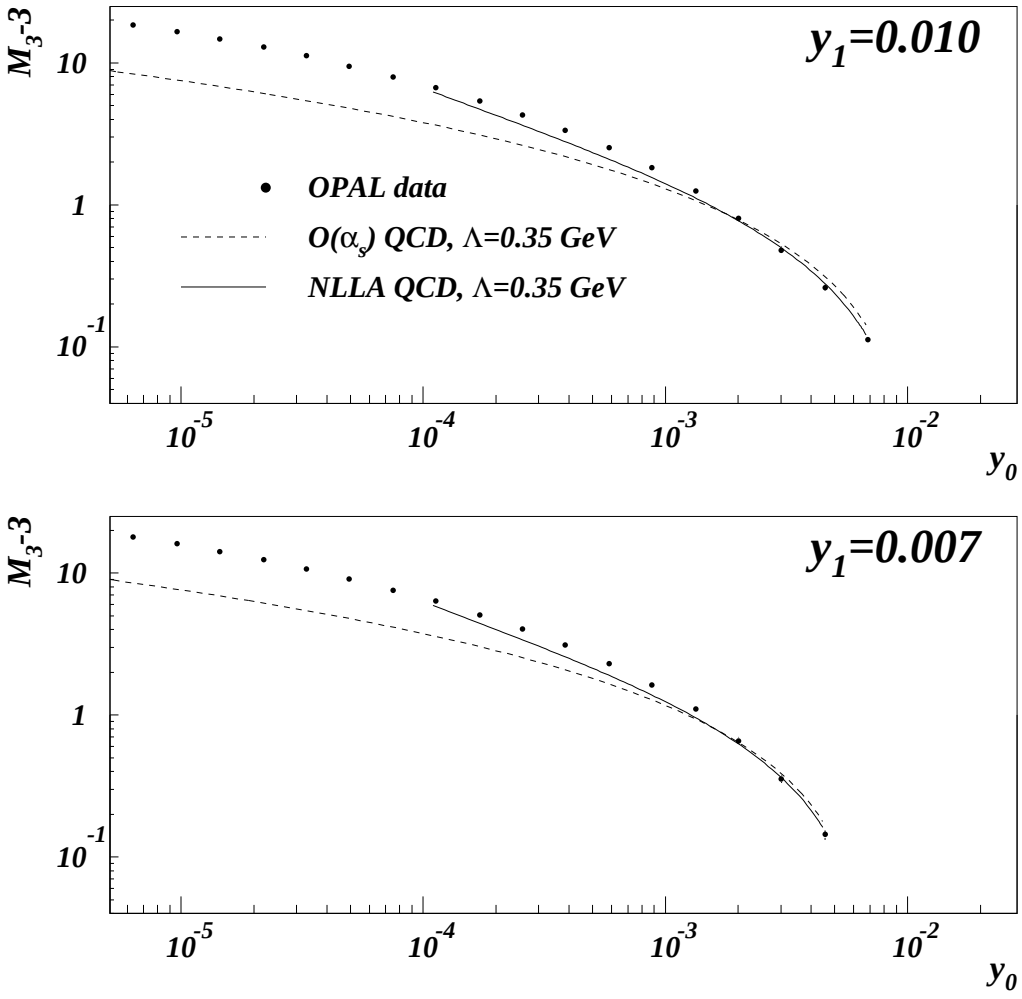

Figure 2: Sub-jet multiplicity of three-jet events at two different selection scales, y_1. The solid points represent OPAL data (corrected to hadron level), and the analytic QCD calculations are shown as curves.

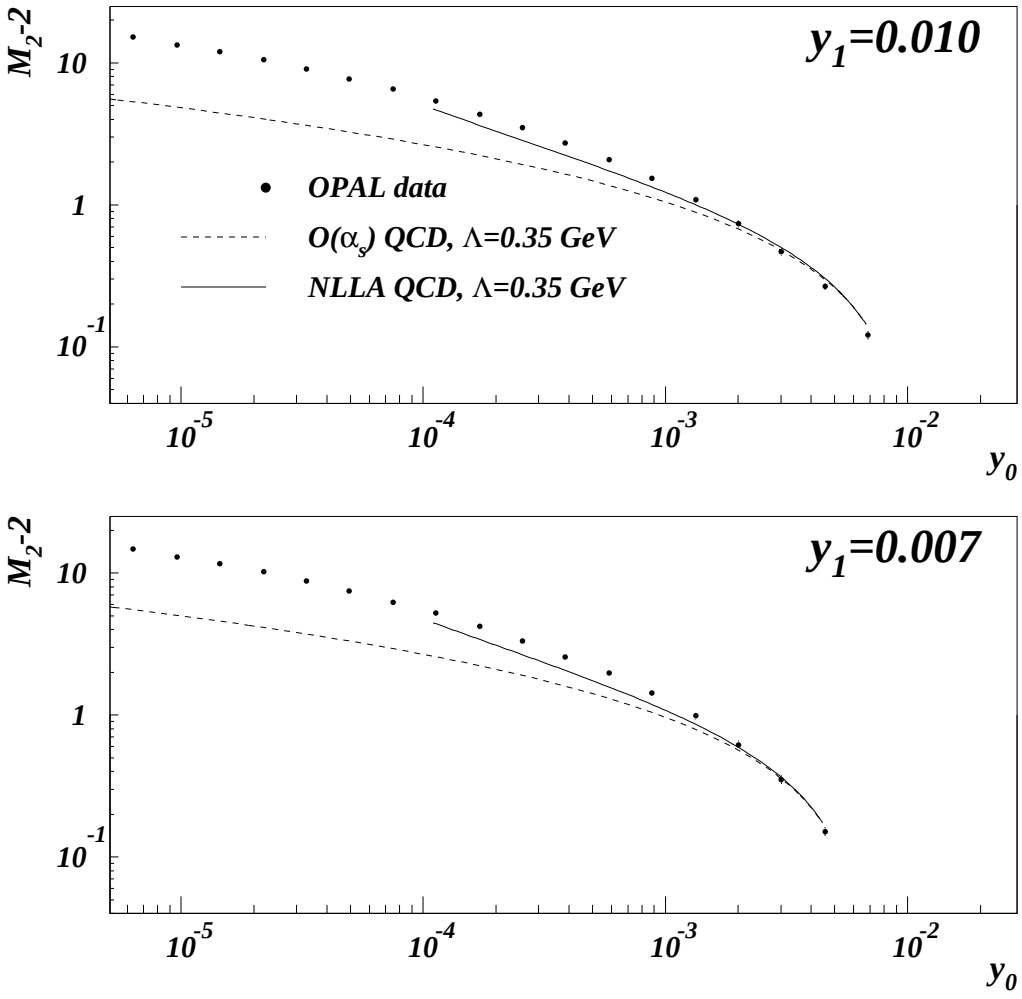

Figure 3: Sub-jet multiplicity of two-jet events at two different selection scales, y_1. The solid points represent OPAL data (corrected to hadron level), and the analytic QCD calculations are shown as curves.

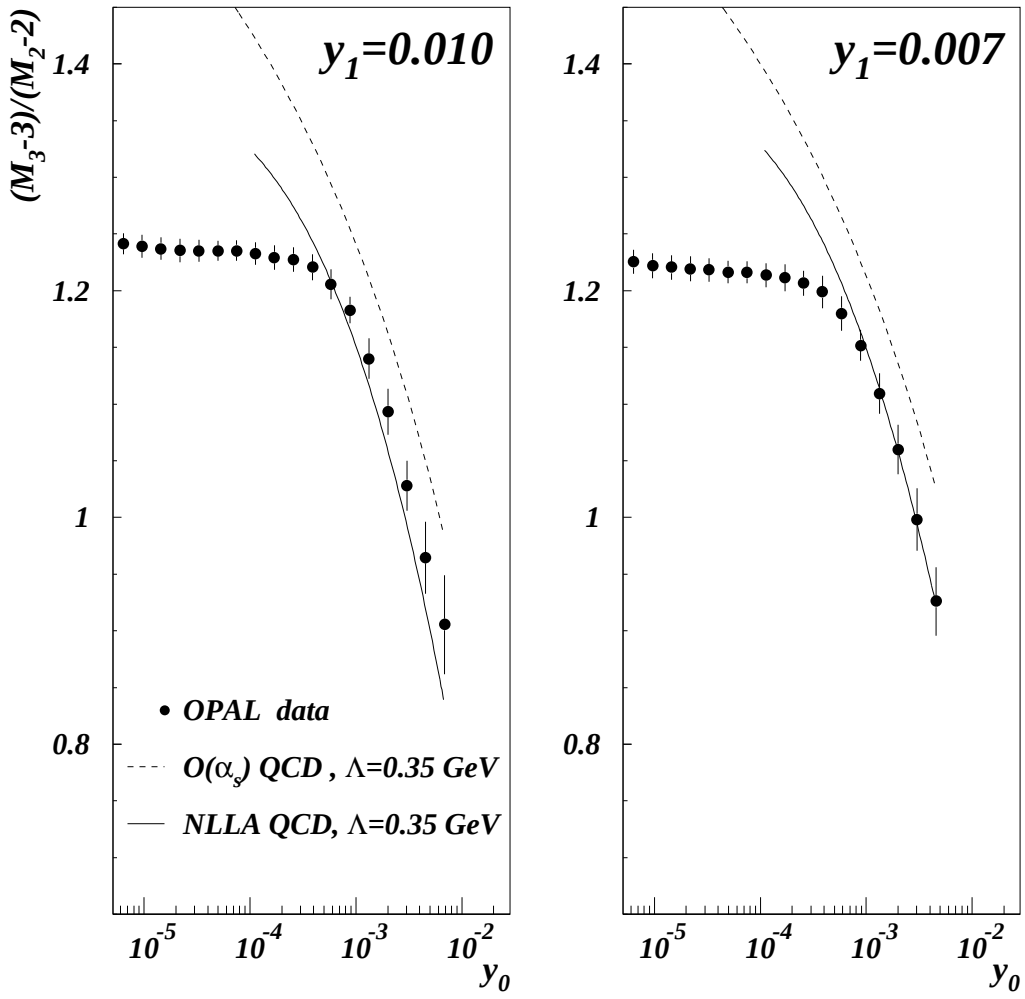

Figure 4: Ratio of sub-jet multiplicities in three-jet and two-jet events, after subtraction of the initial number of jets. The solid points represent OPAL data (corrected to hadron level), and the analytic QCD calculations are shown as curves.

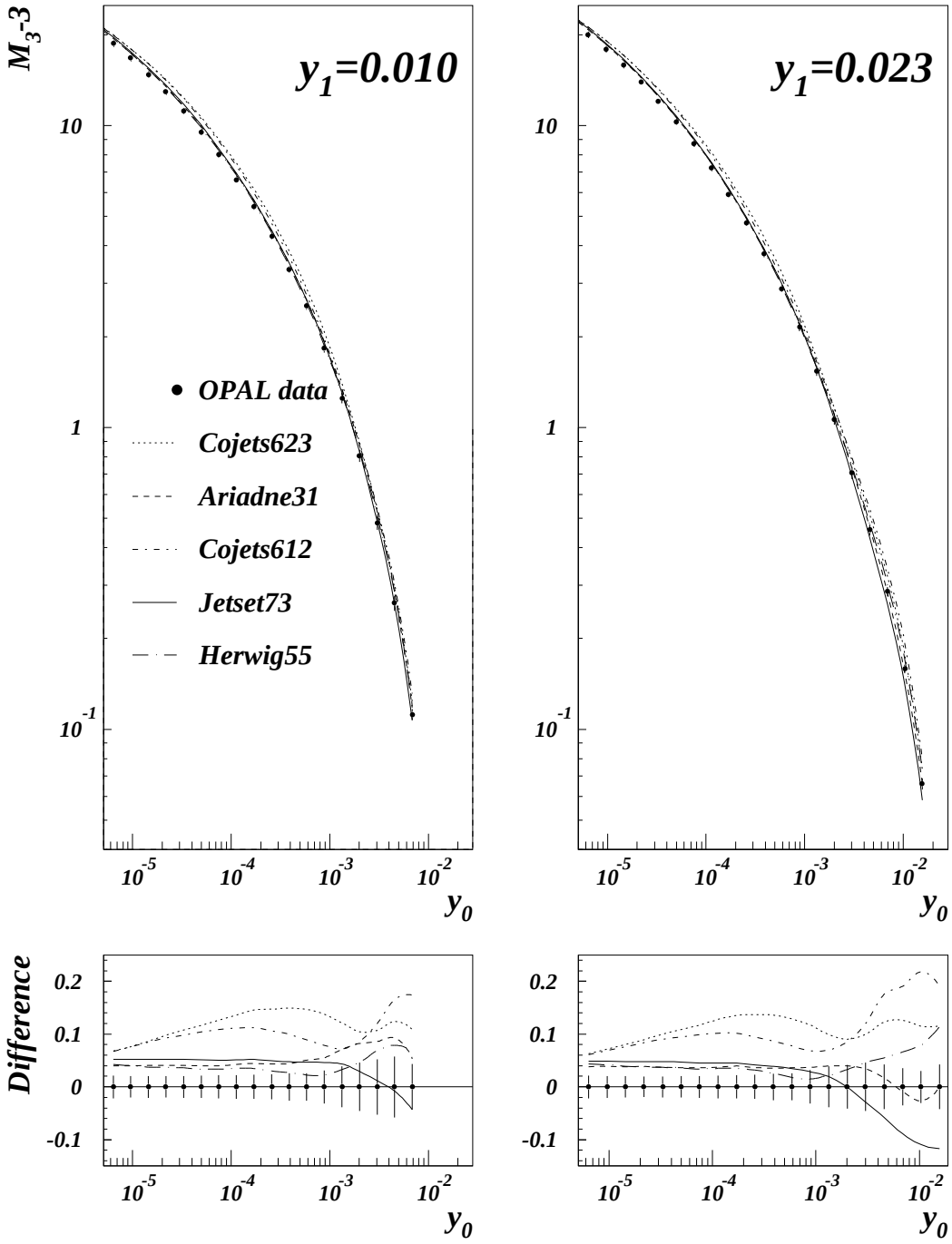

Figure 5: Sub-jet multiplicity of three-jet events at two different selection scales, y_1. The solid points represent OPAL data (corrected to hadron level), and the predictions of various Monte Carlo models are shown as curves. The fractional difference between models and OPAL data is shown, with the combined statistical and systematic uncertainties on the data shown as points with error bars.

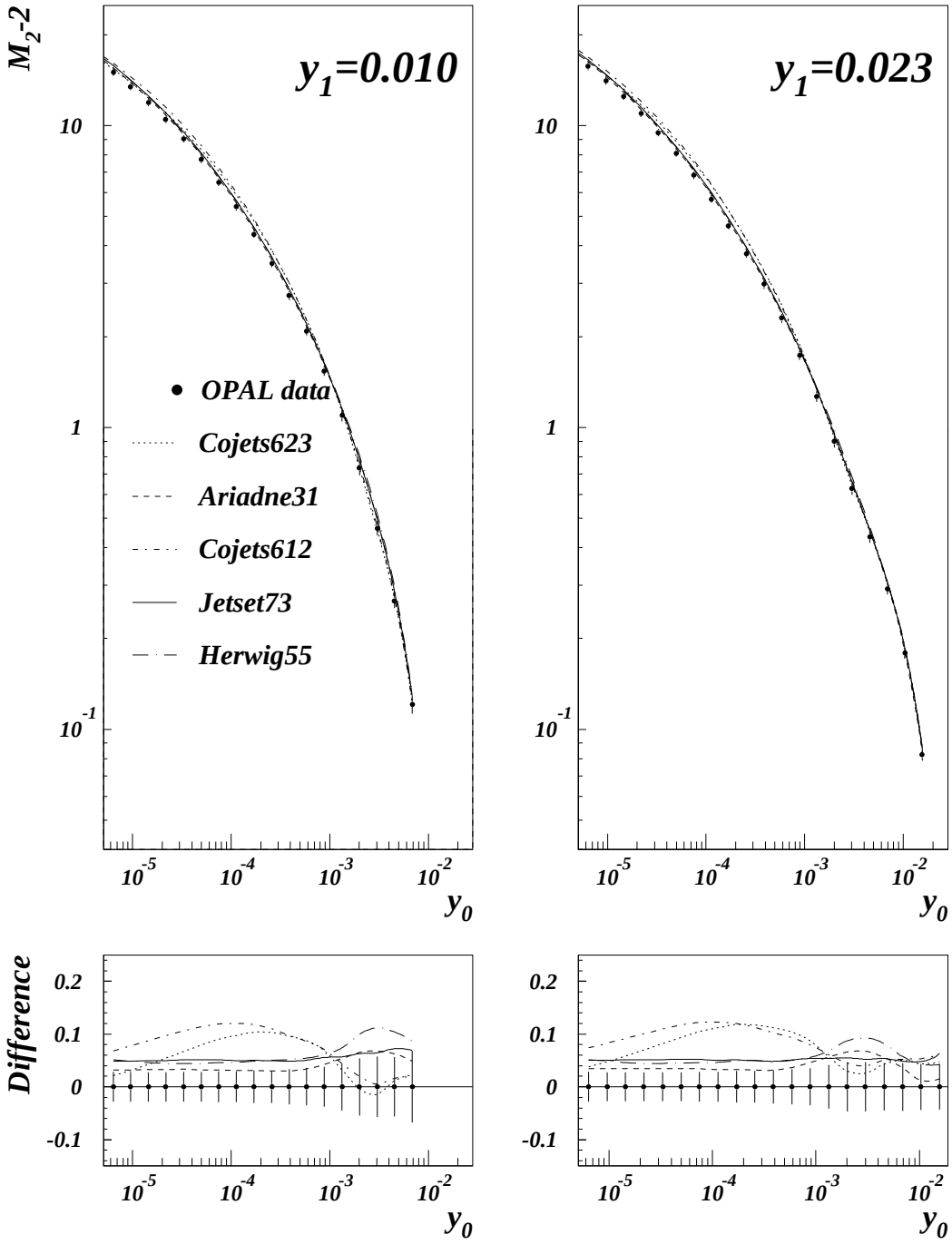

Figure 6: Sub-jet multiplicity of two-jet events at two different selection scales, y_1. The solid points represent OPAL data (corrected to hadron level), and the predictions of various Monte Carlo models are shown as curves. The fractional difference between models and OPAL data is shown, with the combined statistical and systematic uncertainties on the data shown as points with error bars.

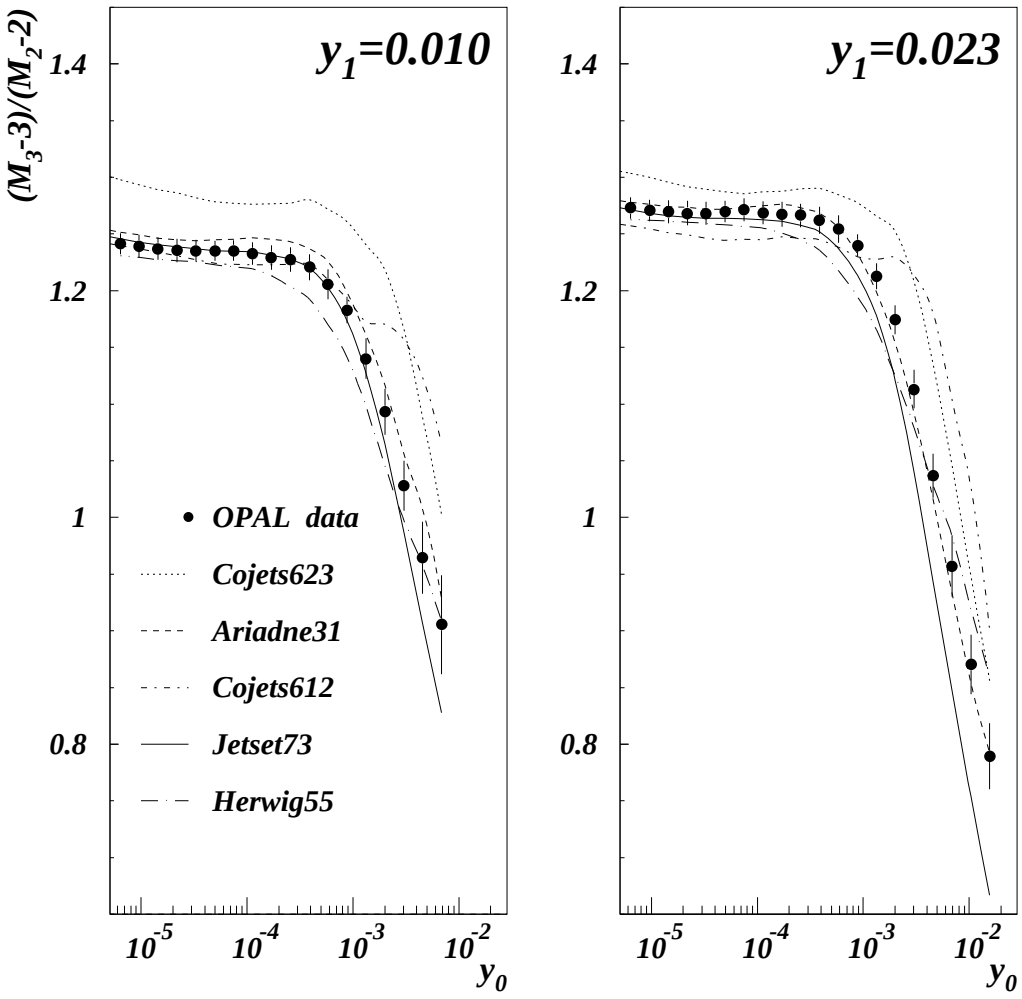

Figure 7: Ratio of sub-jet multiplicities in three-jet and two-jet events, after subtraction of the inital number of jets. The solid points represent OPAL data (corrected to hadron level), and the predictions of various Monte Carlo models are shown as curves.

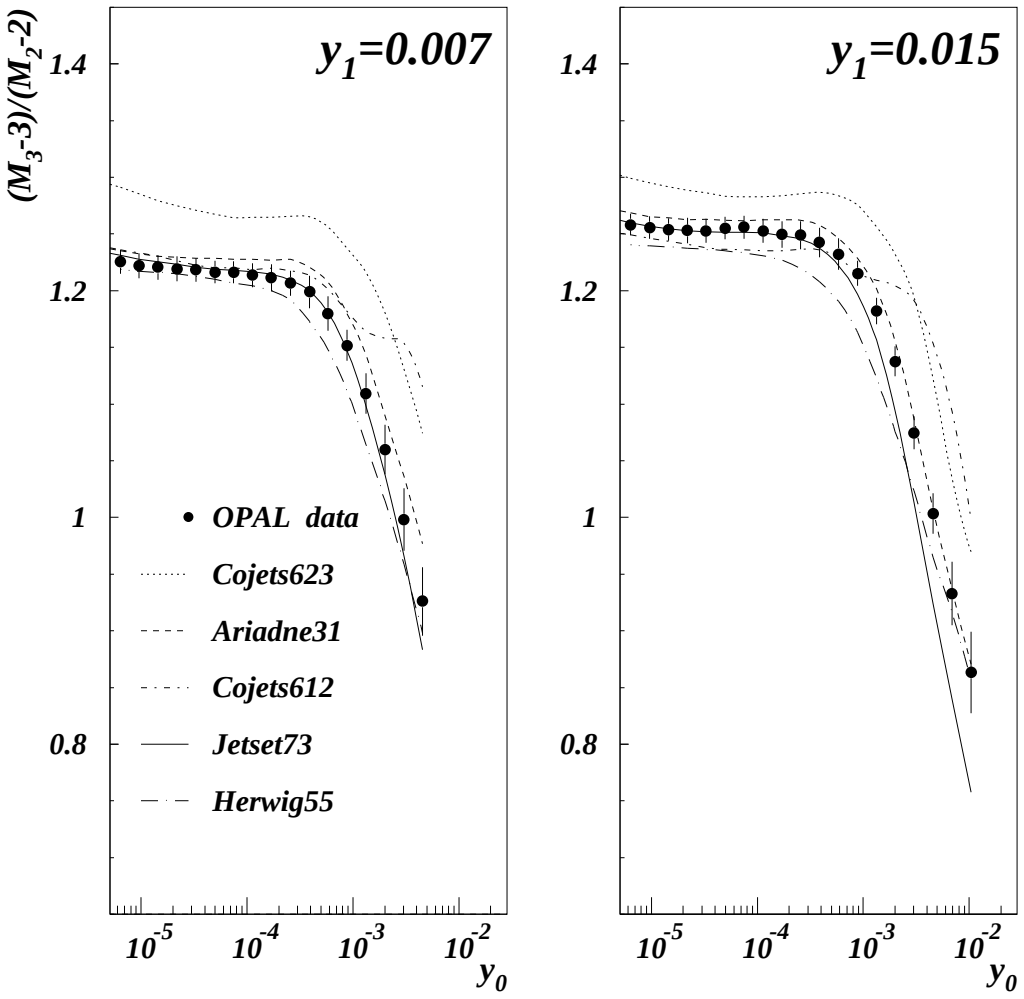

Figure 8: Ratio of sub-jet multiplicities in three-jet and two-jet events, after subtraction of the initial number of jets. The solid points represent OPAL data (corrected to hadron level), and the predictions of various Monte Carlo models are shown as curves.

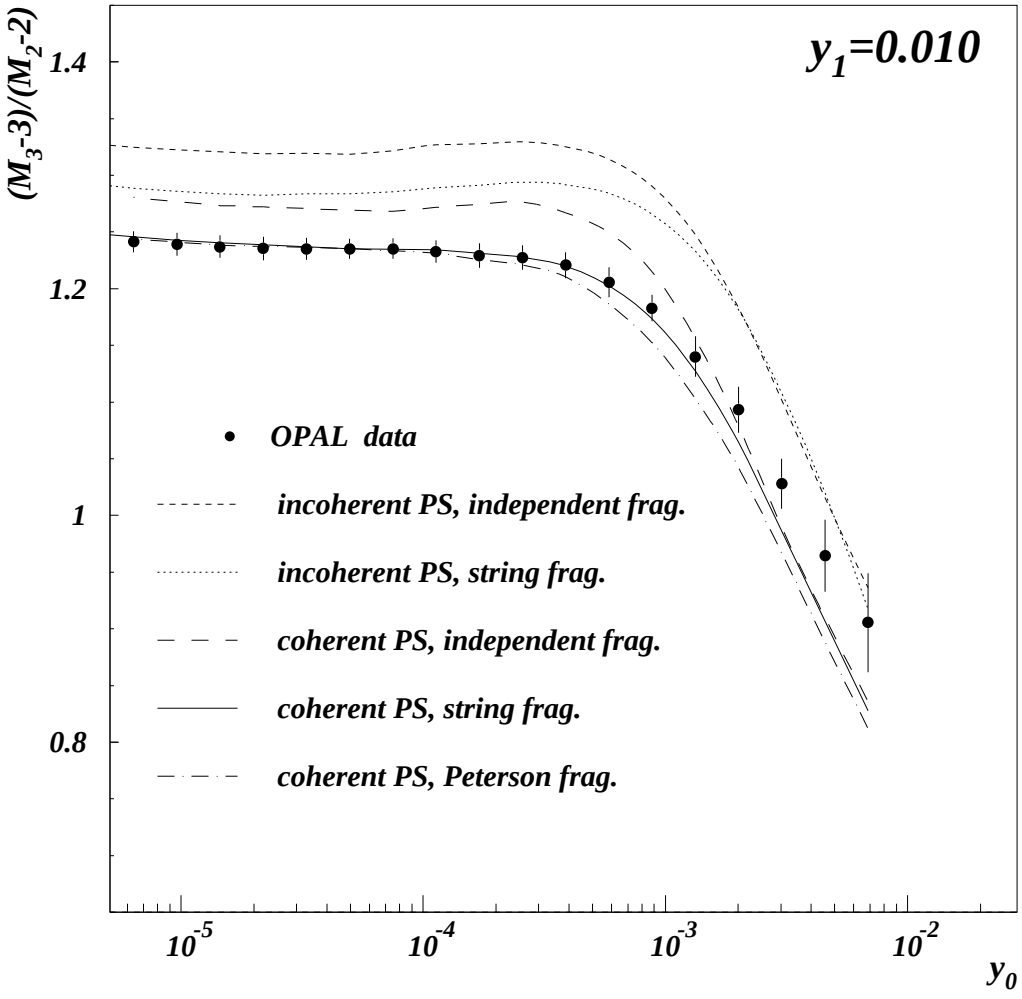

Figure 9: Ratio of sub-jet multiplicities in three-jet and two-jet events, after subtraction of the initial number of jets. The solid points represent OPAL data (corrected to hadron level), and the predictions of various JETSET Monte Carlo models of hadronisation and fragmentation are shown as curves.